Journal of Archaeological Science (2003) **30,** 123–133
doi:10.1006/jasc.2002.0813, available online at http://www.idealibrary.com on IDEAL®

ESR Dating of Tooth Enamel From Aterian Levels at Mugharet el 'Aliya (Tangier, Morocco)

P. J. Wrinn*

Department of Anthropology, Box 210030, University of Arizona, Tucson, AZ 85721-0030, U.S.A.

W. J. Rink

School of Geography and Geology, McMaster University, 1280 Main St. W., Hamilton, Ontario, Canada L8S 4M1

(*Received 4 December 2001, revised manuscript accepted 24 January 2002*)

Electron spin resonance (ESR) dating has been carried out on ungulate tooth enamel samples from the Pleistocene deposits of Mugharet el 'Aliya, Atlantic coastal Morocco. Age estimations for wave-induced breaching of the cavity and initial sand deposition (Layer 10) are 62 ± 6 ka BP by the Early Uptake (EU) model and 81 ± 9 ka BP by Linear Uptake (LU). Samples from Aterian occupations in Layers 5 and 6 and a possible occupation in Layer 9 yielded EU estimated ages between 39 ± 4 and 44 ± 5 ka BP and LU ages between 47 ± 5 and 56 ± 5 ka BP. Incorporating the entire range of EU and LU model ages, the Aterian occupations are dated to between 35 and 60 ka BP. When compared with the published, mostly radiocarbon-based ca. 40–20 ka BP chronology for the Moroccan Aterian (e.g., Debénath, 1992), these new results imply an Aterian arrival or Mousterian-to-Aterian transition occurring beyond the upper limit of the radiocarbon method.

Keywords: ELECTRON SPIN RESONANCE, CHRONOMETRIC DATING, ATERIAN, MIDDLE PALAEOLITHIC, MUGHARET EL 'ALIYA, MOROCCO.

Introduction

In Morocco, more than 60 cave and open-air sites possess Middle Palaeolithic archaeological deposits (Wengler, 1997) (Figure 1). Based on stone artefact typology and technological features, these assemblages have been divided into two facies: Mousterian and Aterian. Traditionally, the Aterian has been classified as an "evolved" end-stage of the local Mousterian, demonstrating greater laminarity and higher proportions of Upper Palaeolithic retouched tool types (e.g., endscrapers and burins) than its predecessor (Bordes, 1976–77). Most significantly, the Aterian is characterized by the presence of classic *fossiles directeurs*: pedunculates and bifacial foliates. A Mousterian-Aterian transitional sequence following these criteria has recently been advanced for the Grotte du Rhafas and Station Météo sites in eastern Morocco, where Aterian and Proto-Aterian deposits directly overlie Mousterian assemblages (Wengler, 1985–86, 1997). Studies of hominid fossils from Mousterian (Jebel Irhoud) and various Aterian localities in Morocco provide further support for a model of gradual, local evolution of early anatomically modern human groups during the late Middle and Upper Pleistocene (Hublin, 1993).

The absolute chronology for the Middle Palaeolithic in this region is less certain. Five electron spin resonance (ESR) determinations on tooth enamel samples from Jebel Irhoud suggest a Mousterian occupation during Oxygen Isotope Stage (OIS) 6, corresponding to 130–190 ka BP (Grün & Stringer, 1991). However, the Early Uptake (EU) model age estimates range between 90 and 125 ka BP and Linear Uptake (LU) between 105 and 190 ka BP, indicating substantial uncertainty in the age determination, especially given the close stratigraphic association of the enamel samples (Hublin, 1993). The Aterian, represented at many more sites in the Maghreb, is generally assigned to the period between 40 and 20 ka BP on the basis of numerous radiocarbon and a few thermoluminescence (TL) and optically stimulated luminescence (OSL) dates (Debénath, 1992). Despite the appearance of continuity provided by the archaeological and skeletal evidence, the radiometric ages imply that hominid populations abandoned the region during the first half of the last glacial period. In the Central Sahara, Aterian occupations seem to have much greater

*Corresponding author. E-mail: pwrinn@u.arizona.edu

0305–4403/03/$-see front matter

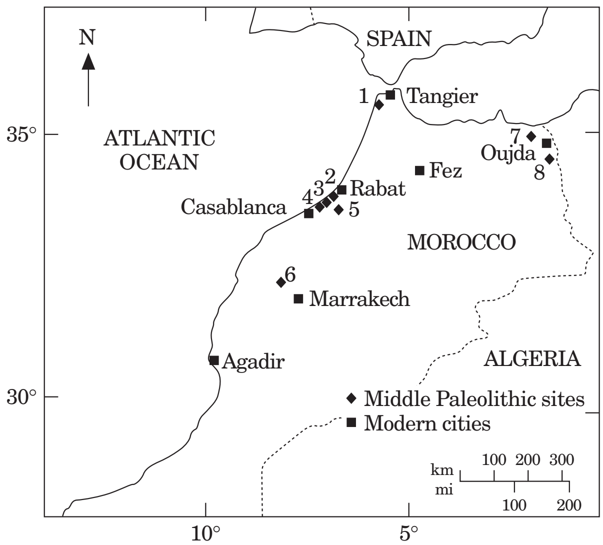

Figure 1. Map of Morocco showing sites mentioned in the text. 1. Mugharet el 'Aliya, 2. Dar es Soltan I and II, 3. Grotte Zouhrah, 4. Grotte des Contrabandiers, 5. Chaperon Rouge, 6. Jebel Irhoud, 7. Taforalt, 8. Grotte du Rhafas and Station Météo.

antiquity; TL and OSL dates on Aterian-bearing sands from cave sites in the Tadrart Acacus (Libyan Sahara) range between 90 and 60 ka BP (Cremaschi *et al.*, 1998). Aterian artefacts recovered from numerous ancient Saharan lake bed contexts, such as at Adrar Bous (Clark, 1993), are probably of similar age, for abundant ^{230}Th/^{234}U determinations (e.g., Fontes & Gasse, 1991) on desert lacustrine carbonates designate several humid episodes between 150 and 75 ka BP, followed by a hyperarid period in the Sahara lasting until *c.* 12 ka BP (Wendorf & Schild, 1992). Given this evidence, one could reasonably anticipate the appearance of Aterian groups in Morocco (1) during later phases of the Last Interglacial (OIS 5), at which time there is clear evidence for the Aterian in humid regions of the Sahara, or (2) in the early stages of the succeeding glacial period (OIS 4), when the onset of hyperaridity may have forced Aterian groups to abandon the Sahara and migrate toward more resource-rich valley and coastal zones to the north and west. Either scenario would support the existence of pre-40 ka BP Aterian deposits in Morocco.

The current Maghreb Aterian chronology also implies that Middle Palaeolithic technology lingered very late in Morocco. By comparison, the latest Middle Palaeolithic in southern Spain, associated with Neanderthal remains, has been dated by ^{230}Th/^{234}U (teeth) and ^{14}C (bone) between 34–27 ka BP (Hublin *et al.*, 1995), while charcoal AMS dates from early Upper Palaeolithic contexts on Gibraltar indicate a range of 31–28 ka BP (Barton *et al.*, 1999). Some authors have associated the Middle Solutrean complex of the Iberian Peninsula with Aterian migrants from northwest Africa, citing similar-looking pedunculates and bifacial foliates and ages seemingly coincident with the latest dated Aterian deposits (e.g., Pericot, 1942; Debénath *et al.*, 1986; Otte, 1997; Bouzouggar *et al.*, in prep.). This position has faced criticism on both technological and chronological grounds (for a thorough recent review, see Straus, 2001).

The extended occupation hiatus and very late survival of the Middle Palaeolithic in Morocco may be more apparent than real, reflecting limitations with the dating techniques employed. Most of the Aterian radiocarbon dates are conventional and derived from bulk samples of marine and terrestrial shell, bone, or carbonaceous earth, materials particularly susceptible to contamination (Aitken, 1990). Recrystallization, open-system carbon exchange, or minimal sample pretreatment may all result in significant underestimations of true age. In addition, a number of the dates are infinite, implying that some Aterian deposits may lie beyond the upper limit of the radiocarbon method. There is thus considerable ambiguity in the absolute Aterian chronology that could be confronted through the application of alternative dating techniques. In this paper, we present new ESR results on ungulate tooth enamel from stratified Aterian deposits at Mugharet el 'Aliya, a limestone cavity on the Atlantic coast of northwestern Morocco.

Background

One of the "Caves of Hercules", Mugharet el 'Aliya is located at Cap Ashakar (35°45′N, 5°56′W), approximately 4 km south of Cap Spartel and 11 km southwest of Tangier, Morocco (Figure 1). It formed as an internal cavity by groundwater dissolution of the surrounding Upper Pliocene (Alouane, 1997) conglomeratic limestone outcrop. The chamber was subsequently breached by wave action during a high sea level phase (Howe, 1967), an event probably dating to the Last Interglacial (OIS 5). Associated with the cave breach, an uneven terrace of limestone rockfall filled with cemented beach deposits extends from within the cave entrance 5–10 m west toward the ocean. A single uncorrected ^{230}Th/^{234}U determination on shell fragments from these cemented beach deposits, considered Ouljian or Last Interglacial in age according to the Moroccan marine sedimentary sequence (e.g., Weisrock *et al.*, 1999), yielded a date of 125 ± 10 ka BP (Stearns & Thurber, 1965). At the base of the rockfall, a low (5–6 m above mean sea level) marine limestone platform, formed as waves cut into and eroded the rockfall deposits during a more recent high sea level phase (i.e., mid-Holocene), extends an additional 15–20 m west to the edge of the water. Presently, the cave entrance lies 18 m above sea level, 6 m below the top of the limestone outcrop hosting the cavern. The chamber is approximately 15·5 m long and 12 m wide, with a west-facing entrance.

Amateur excavators from Tangier conducted sporadic excavations at Mugharet el 'Aliya between 1936

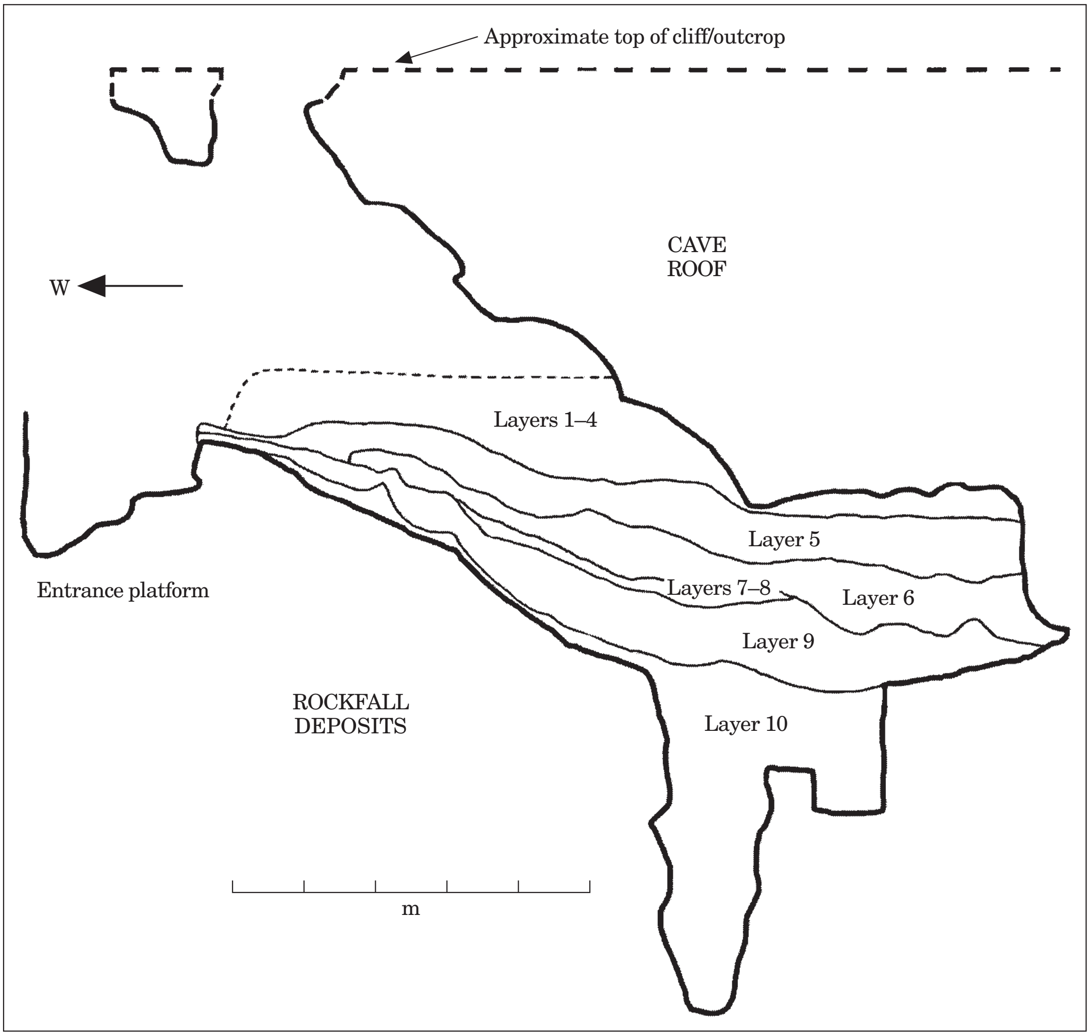

Figure 2. 1947 Section of Mugharet el ‘Aliya. Redrawn and simplified from Howe (1967: Figures 40 and 42).

and 1938, clearing most of the recent and Neolithic deposits (see Gilman, 1975). In 1939, Carleton Coon of Harvard University began a systematic study of the Pleistocene levels (Coon, 1957) and provided training in excavation methods to the amateurs, who continued the work through 1940 (Howe & Movius, 1947). Bruce Howe (Harvard University) and Charles Stearns (Tufts University) visited the site in 1947 to collect soil samples and study the stratigraphy, concluding research at the site (Howe, 1967). All of the excavated material is now stored at the Peabody Museum, Harvard University, Cambridge, U.S.A. Nearly all of the sediment was removed from the chamber during excavation, and Mugharet el ‘Aliya has recently been converted into a café.

Stratigraphy

The Pleistocene deposits were described by Stearns (Howe, 1967: 27–35, 95–110) (Figure 2), whose work guided our interpretation of the local palaeoclimate. Based on the 1947 stratigraphic profile, he defined five units composed predominantly of fine- to medium-grained, well sorted sands. All of the deposits were of eolian origin, derived from beaches that repeatedly formed outside the cave during low sea level phases of the last glacial cycle. Differences in the colour and texture of the sediments therefore reflected conditions within the cave during and after deposition.

Beginning with the lowest Layer 10, here we describe the lithology of the sedimentary deposit:

Layer 10: Cemented sand (includes “Layer 11” in Howe, 1967)

This layer consisted of yellow-white beach sand and well-rounded pebbles deposited shortly after the chamber was breached by wave erosion. The rockfall debris altered the configuration of the original cavity floor, producing a “new” floor sloping steeply downward from the northwest to the southeast sectors of the chamber (Figure 2). Therefore, these deposits were confined to the back, southern end of the cave with thickness between 0·05 and 4·5 m. The sand may have been deposited during climatic conditions comparable to those in the area today. Subsequently, the sand was cemented through interaction with carbonate-rich groundwater. There were some areas of unconsolidated sand (defined as "Layer 11" in Howe, 1967), separated from the cemented portions by thin, black manganese and iron oxide crusts. The deposit was capped by travertine layer 0·02–0·05 m thick, indicating a period of high cave humidity and somewhat warmer external temperatures.

Layer 9: Red sand 2

This layer was defined by red, clayey sand. Though loose in the centre of the chamber, it was cemented by calcium carbonate deposits along the cave walls and adjacent to the entrance platform. Yellowish beach sand was probably deposited during a cool, low sea level phase, and then subsequently weathered and rubified during a warmer period with increased precipitation. Thickness varied from 0·05 m near the entrance platform to 1·2 m in the southeast corner of the cave.

Layers 8 and 7: Grey and orange sands

These discontinuous lenses of loose sand had thicknesses between 0·05 m and 0·80 m. They were interspersed by crusts of calcium carbonate, particularly along the cave walls and near the entrance platform. Calcite weathering and crust formation similar to the top of Layer 10 imply high cave humidity and relatively warm, wet outside conditions.

Layer 6: Brown sand

This layer consisted of brown, clayey, sand of uniform texture deposited when the sea level was lower than today. Retention of iron oxides and formation of secondary carbonate nodules imply cool, dry depositional conditions within the cave, although there was some cementation along the walls. Thickness varied from 0·10 m in the northern end of the cavity to 1·6 m in the central and southeast zones.

Layer 5: Red sand 1

This loose-to-consolidated red sand closely resembled Layer 9, and also weathered and rubified after deposition during a warmer, wetter climatic regime. Associated with this weathering, discontinuous calcium carbonate crusts formed in the deposit, especially along the walls and near the cave mouth. The deposit varied in thickness from 0·50 m (northern end of cave) to the 1·4 m (central region).

Layers 4–1: Holocene deposits

Based on the recollections and photographs of the amateur excavators, these sandy layers were bedded horizontally to a maximum thickness of 1·7 m. Layer 4 contained Cardial and Channeled Ware (Neolithic) ceramic fragments, animal bones, and stone tools as well as a human child's skull within charcoal-rich sediment. Layer 3 was a thin, discontinuous carbonate crust, while Layers 2 and 1 yielded a mixture of Roman, Mediaeval and recent artefacts (Howe, 1967: 103–104).

According to Stearns, Pleistocene deposition proceeded in three major phases: Layer 10, Layer 9, and Layers 6 and 5. Each of these phases was associated with a sea level lower than that found outside the cave today, allowing eolian deposition of beach sands. This setting would be consistent with sea levels during stadial periods of the last glacial cycle. Following this model, Layers 6 and 5 should be considered a single depositional unit. The red colour of Layers 5 and 9 is the result of post-depositional weathering processes in the soil related to increased ground water circulation and calcium carbonate precipitation, linked to a wetter environment within the cave. Thin travertine deposits bracketed the top and bottom of Layer 9 and occurred in small lenses near the walls and dripline (cave entrance) in the upper layers, suggesting repeated instances of locally higher moisture and cooler temperatures than today. The rubification and carbonate deposition phases could be associated with interstadial periods, during which there was little or no sand deposition. Layers 8 and 7, discontinuous deposits representing a time of carbonate crust formation and limited aeolian contribution, might have marked a transitional phase from humid to drier and colder local conditions.

Archaeological Content

The Middle Palaeolithic stone artefacts from Mugharet el 'Aliya were described by Howe (1967: 110–146). Based on museum archive records, recollections of B. Howe (personal communication, 1997), and several instances of missing or empty artefact boxes noted during examination of the collection by one of us (PJW), there have evidently been some losses, both of tools and debitage, during museum storage. The extant portion of the original assemblage held at the Peabody Museum has recently been reanalysed by Bouzouggar *et al.* (in prep.). An isolated core found in an area of unconsolidated sand in Layer 10 was undoubtedly intrusive from overlying deposits. Layer 9 yielded a small assemblage (Bouzouggar *et al.*, report 23 artefacts, to 54 in Howe) including sidescrapers, retouched blades, and two oval bifacial foliates. The foliates were recovered near the upper surface of Layer 9, leaving open the possibility that they were intrusive from adjacent Layer 6. Crusts and brown-coloured sediment adhere to several more of the artefacts, leaving only a handful assigned with confidence to Layer 9 by Howe (1967: 144); so scanty is this assemblage that it may reflect sediment reworking by porcupines (see below) or groundwater rather than hominid occupation. The 13 lithics from Layer 7 may similarly have been intrusive from above.

By contrast, Layers 6 and 5, yielding 750 and 431 lithic remains, respectively (Howe, 1967; Bouzouggar *et al.*, report 472 and 10 lithic artefacts, respectively), display a clear Aterian affinity. The extant Layer 6 assemblage includes numerous bifacial foliates and sidescrapers, a few pedunculates, and several blades, Mousterian points and endscrapers, all on high-quality, local flint. According to Howe (1967), Layer 5 yielded proportionally fewer foliates and more Middle Palaeolithic tools (e.g., sidescrapers, Mousterian points) than Layer 6, but the assemblages are otherwise comparable, supporting the premise that the two layers represent a single depositional series or occupational sequence. Bouzouggar *et al.* (in prep.) report evidence of the *linéale* Levallois method (Boëda *et al.*, 1990), whereby a single large flake (*éclat préférentiel*) is removed from a radially and (in this case) bifacially prepared core. Some cores continued to be rejuvenated and exploited by this method until they were quite small (<3–4 cm). In addition, rare blades found in the Layer 6 assemblage were removed from opposed platform cores, and some of the smaller cores became discoid in the final phase of reduction. Cortical flakes are rare and retouched pieces (tools, flakes, and flake fragments) comprise >60% of the total lithic material in these layers (Howe, 1967: 112), suggesting that Mugharet el 'Aliya may have been repeatedly occupied for short episodes by mobile Aterian forager groups employing a highly curated toolkit (e.g., Binford, 1979). However, the selectivity of the collection places significant constraints on such inferences. Small debitage fragments were not regularly saved during excavation (B. Howe, personal communication, 1997).

The Pleistocene faunal material has recently been analysed by Wrinn (in prep.). All bone fragments were apparently saved during the Coon phase of the excavation (Coon, 1957: 61), yet it is clear that during succeeding phases and/or museum storage, a substantial portion of the small splinters and "unidentifiable" shaft fragments was thrown away. However, the existing collection is undoubtedly more complete, especially with respect to teeth (B. Howe, personal communication, 1997), than is the case for the lithic artefacts. Out of more than 3800 identifiable specimens, 29 animal taxa were recorded, including at least three species of gazelle, zebra, wild cattle, *Pelorovis*, hartebeest, warthog, golden jackal, and spotted hyena. Hyena coprolites and teeth from juvenile hyenas indicate that denning occurred intermittently throughout the depositional history of Mugharet el 'Aliya. The assemblage from Layer 9 shows the strongest signature for collection by carnivores and possibly porcupines.

Table 1. Locations and taxonomic designations of Mugharet el 'Aliya tooth samples

McMaster sample no.	Harvard ID	Archaeological layer	Taxon
97123a	NWC.R1B/234	5	Bovid
97122a	NEB.BR?/218	6	Bovid
97121a	1.K.R2/25	9	Bovid
97120a	1.10(BC)	10	Equid

At the same time, there is a sharp decline in taxonomic evenness between the lower Layers 10 and 9 and the upper Layers 6 and 5, with the latter deposits overwhelmingly dominated by gazelle remains. This shift in the faunal composition may reflect the arrival of Aterian forager groups coupled with increasing overall aridity in the region.

Hominid remains discovered at Mugharet el 'Aliya include three isolated teeth and a juvenile maxilla containing three teeth (Şenyürek, 1940). None of the fragments was found *in situ*, but fluorine analysis of a sample of the maxilla produced a fluorine/phosphate ratio consistent with animal bones from Layer 5 (Howe, 1967: 143). Initially assigned to *Homo neanderthalensis* (Şenyürek, 1940), the maxilla shares morphological characters in common with specimens from other Aterian localities (e.g., Dar es Soltan II, Grotte des Contrabandiers, Grotte Zouhrah) (Hublin, 1993), and has recently been reassigned to early anatomically modern human (*Homo sapiens* Subspecies indet.) (Minugh-Purvis, 1993).

ESR dating

Sample preparation and experimental methods

The ungulate tooth enamel samples were taken from the Peabody Museum collection during the course of the faunal analysis (Wrinn, in prep.). They were sourced from each of the principal Pleistocene sediment layers (Table 1); Figure 3 gives approximate sample locations on the plan view. It should be emphasized that each sample had adhering sediment of the colour and composition appropriate to the assigned layer. The enamel on the teeth was in excellent condition with a pristine white colour. The teeth were prepared according to the protocol given in Rink (1997). The sediments attached to the teeth were heavily cemented. Sediments located less than 3 mm away from the enamel surfaces on the tooth were analysed for their U, Th and K concentrations, and used to determine the beta and gamma dose rates to the enamel from sediment, except for sample 97121a, where sediment recovered from the same stratum was used for the calculation. In this site, where the sediment is primarily sandy without a large contribution from

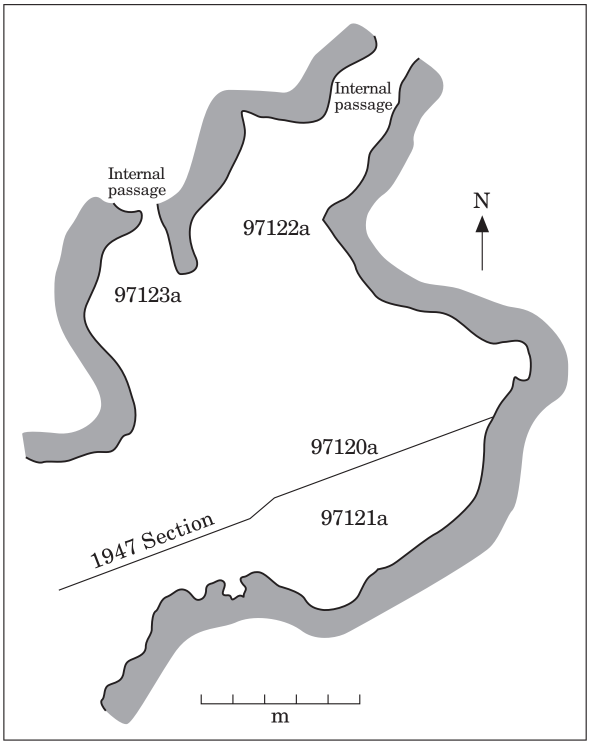

Figure 3. Plan of Mugharet el 'Aliya, showing 1947 section and approximate locations of ESR samples. Adapted from Howe (1967: Figure 43).

limestone elements, it was suspected that the dose rates derived from sediment attached to teeth should give reasonably accurate estimates of the bulk gamma dose rates.

The ages were calculated using the software ROSY version 1.41 (Brennan *et al.*, 1999). This program includes new beta attenuation calculations (Yang *et al.*, 1998) based on One-group theory which have recently been used in a number of ESR dating studies. The alpha dose rates were determined using the option "Varies with energy". An initial $^{234}U/^{238}U$ ratio of 1·4 was assumed in the age calculations. The density of the cementum, dentine and enamel were based on the average values of Rink & Hunter (1998): 2·54, 2·82 and 3·00 g cm^{-3}, respectively. The density of the sediment was assumed to be 2·00 g cm^{-3}. We used uncertainties of $\pm$ 10% of the density value in all cases. The moisture contents of the cementum, dentine and enamel were assumed to be 5 $\pm$ 5%, 5 $\pm$ 5% and 0 $\pm$ 0% respectively. The U, Th and K concentrations in sediment and the U concentrations in dental tissues were determined using neutron activation analysis at the McMaster Nuclear Reactor. The samples were irradiated using a ^{60}Co gamma radiation source to the following dose levels: 10, 20, 40, 80, 120, 160, 240, 320, 480 Gy. The g=2·0018 ESR signal intensity data was fitted with a single saturating exponential function using 1/intensity^2 weighting. The error in the gamma equivalent dose was determined following the approach of Brumby (1992). The software V-Fit (courtesy of E. Bulur) was used for the fitting and error calculations.

The moisture contents of the sediment could not be measured using fresh samples, thus the ages were calculated using three different geologically reasonable values: 0%, 10 $\pm$ 10% and 20 $\pm$ 10%. These values and their uncertainties were used to calculate beta sediment dose rate, and the values plus a 20% error in the dose rate value were used to reconstruct the gamma dose rate.

The gamma, beta and alpha dose rates to the teeth were significant but moderate, making the contribution from cosmic radiation more significant than in other settings. Because of this a detailed analysis of the geometry of the cave roof and the overlying sediments was needed to determine a reasonably accurate assessment of the shielding geometry above the teeth. The cosmic dose rate to the samples was reconstructed using a combination of the approximate sample locations on the plan view (Figure 3) and the cross section showing the thickness of the cave roof in Figure 2. Samples 97120a and 97121a come from the rear part of the cave, while 97122a and 97123a come from areas closer to the front of the cave, near openings to much smaller cavities in the limestone (Figure 3).

The cosmic dose rates were calculated using the data of Prescott & Hutton (1988) as incorporated in the ROSY version 1.41 software program. This calculation is based on a shielding geometry corresponding to a layer of overburden of uniform thickness and which extends to the horizon in all directions. However, in the cave nearly all of the shielding is due to the overburden of cave roof that lies away from the entrance and landward of the cave. This limestone has an approximate thickness of about 8 m. To correct for the fact that this overburden does not continue seaward, the calculation is made using the half-thickness of the cave roof that extends landward. Thus a shielding of 4 m was used as the shielding attributable to limestone overburden for all samples, since even the samples toward the rear of the cave receive negligible shielding seaward.

The sediment thicknesses above the samples must also be considered in the shielding geometry. As the sediments accumulated over the history of burial this thickness was changing significantly. To accommodate this, we have assumed that the average sedimentation rate was constant, which yields an approximation that the average overburden above each sample was 50% of that encountered at the time of excavation. The total shielding for each sample was then calculated as the sum of 50% of the sediment overburden plus 4 m associated with the roof. Considering all four teeth, the cosmic dose rate makes up 12 to 21% of the early uptake total dose rates, and 16 to 24% of the linear uptake total dose rates.

Table 2. Analytical data on dental tissues and sediments

McMaster sample no.	D_E (Gy)	U En (ppm)	U Den (ppm)	U Cem (ppm)	U Sed (ppm)	Th Sed (ppm)	K Sed (Wt%)	Enamel thickness (µm)	Sed side rem (µm)	Dentine side rem (µm)
97123a	25·30	1·08	3·80	—	0·66	1·64	0·09	1470	80	46
	(0·43)	(0·1)	(0·1)		(0·1)	(0·11)	(0·01)	(91)	(40)	(23)
97122a	20·20	0·54	3·34	—	0·60	2·53	0·11	1408	65	86
	(0·53)	(0·1)	(0·1)		(0·1)	(0·11)	(0·01)	(90)	(33)	(43)
97121a	18·20	0·29	3·79	—	1·02	1·14	0·05	1152	45	35
	(0·31)	(0·1)	(0·1)		(0·1)	(0·10)	(<0·01)	(672)	(22)	(17)
97120a	38·75	0·27	11·71	9·37*	2·14	0·60	0·02	1121	37	35
	(1·35)	(0·1)	(0·1)	(0·10)	(0·1)	(0·12)	(<0·01)	(102)	(18)	(17)

All analytical uncertainties are shown as ± values in parentheses. D_E is equivalent dose; U is uranium concentration; Th is thorium concentration; K is potassium concentration; Sed is sediment; rem is removed. *Thickness of cementum = 920 µm.

Table 3. ESR dating results (ROSY Ver. 1.41) for Mugharet el ‘Aliya

McMaster sample no.	γ Dose rate (µGy/a)	Cosmic dose rate (µGy/a)	β Sed dose rate (µGy/a)	EU α-En dose rate (µGy/a)	EU β-En dose rate (µGy/a)	EU β-Den dose rate (µGy/a)	EU* Total dose rate (µGy/a)	LU α-En dose rate (µGy/a)	LU β-En dose rate (µGy/a)	LU β-Den dose rate (µGy/a)	LU* Total dose rate (µGy/a)	EU*** Age [ka] (± ka)	LU*** Age [ka] (± ka)
97123a	183	108	24	189	64	32	600	89	31	16	451	42 (3)	56 (5)
97122a	223	108	31	92	31	27	512	42	15	13	432	39 (4)	47 (5)
97121a	189	88	30	52	16	40	413	23	7	19	356	44 (5)	51 (5)
97120a	252	78	6	56	16	132	628*	26	8	64	478**	62 (6)	81 (9)

Ages calculated assuming 10 ± 10% moisture in surroundings throughout the burial period. µGy/a is 1×10^{-6} Gy per year, γ is gamma, β is beta, α is alpha, Den is dentine, En is enamel, Sed is sediment. *Includes a uranium beta dose rate from cementum of 90 µGy/a. **Includes a uranium beta dose from cementum of 44 µGy/a. Reported uncertainty in individual ages is the standard error calculated as the combined effect on ESR age by all sources of systematic and random error, as outlined by Brennan *et al*., 1999.

Table 4. Comparison of ESR dating results using different assumed moisture contents

Sample no.	EU Age (ka)	LU Age (ka)	EU Age (ka)	LU Age (ka)	EU Age (ka)	LU Age (ka)
Moisture content (%)	0	0	10	10	20	20
97123a	41 (3)	53 (5)	42 (3)	56 (5)	43 (3)	58 (5)
97122a	37 (4)	44 (5)	39 (4)	47 (5)	41 (4)	49 (5)
97121a	43 (5)	49 (6)	44 (5)	51 (6)	47 (5)	56 (6)
97120a	59 (5)	77 (8)	62 (6)	81 (9)	64 (6)	85 (9)

Uncertainty in individual age estimates are shown in parentheses after the age value in ka.

Results

The analytical data for the dental tissues and the sediments studied are given in Table 2. The sediments are generally quite low in U, yielding very low gamma dose rates, which though low, are typical of some calcite rich sedimentary environments in caves. The teeth have a low to moderate level of uranium in the enamel and dentine ranging from 0·27 to 1·08 ppm, and 3·80 to 11·71 ppm respectively. The uranium content leads to a spread in the early and linear uptake model age estimates for each single enamel sample. The ESR dating results using an assumed moisture content value of 10 ± 10% are reported in Table 3. The uppermost three teeth yield statistically indistinguishable results for each uptake model used. The Early Uptake (EU) ages ranging from 39 ± 4 to 44 ± 5 ka BP, while the Linear Uptake (LU) ages range from 47 ± 5 to 56 ± 5 ka BP. The stratigraphically lowest tooth yielded significantly older EU and LU ages of 62 ± 6 ka BP and 81 ± 9 ka BP, respectively. The EU and LU age estimates using different assumed moisture contents for individual teeth are statistically indistinguishable (Table 4), primarily because the internal radiation doses from U in the teeth dominate the dose rates to enamel.

Discussion

The variation in age with moisture content is much smaller than the uncertainty in the burial age associated with uranium uptake into the dental tissues for the uppermost and lowermost teeth. The small amount of uranium uptake into the other two teeth (97121a and 97122a) yields EU and LU model ages for each individual tooth that are statistically indistinguishable. Thus these two teeth currently represent the best estimates for possible burial ages in the site. This is the best situation for ESR dating of teeth in a site; when little U-uptake occurs, the precision on the age estimate is mainly influenced by the other sources of error. Since this site is in a maritime setting, the 0% moisture content values are probably not applicable, and for the following discussion we refer to only the age estimates calculated using 10 and 20% moisture (Table 4). Provided that either the EU or LU model is the correct U-uptake model, we can conservatively say, taking into account the other cited sources of uncertainty, that the burial events for tooth 97122a occurred between 35 and 54 ka BP, and that of the next deeper tooth (97121a) occurred between 39 and 62 ka BP.

The other two teeth in the site had considerably larger amounts of U-uptake, giving spreads in the EU and LU model ages that are larger than the uncertainties in those model ages. Uranium series dating of the dentine and enamel in tooth 97123a, and the dentine and cementum in 97120a is underway to refine the true burial ages. However, because of the lower uranium uptake into the teeth situated between them, we can argue on the basis of their stratigraphic position for minimum and maximum age estimates. Thus the uppermost sample must be younger than the age range of 33–53 ka BP, and the deepest sample must be older than the age range of 38–62 ka BP. In order to be certain that this argument is factual, U-series dating is needed to make sure that either the EU or LU model is appropriate for teeth 97121a and 97122a. But if we accept the hypothesis that this is the case for all teeth, as has been proven in many cases for teeth which have been found in limestone caves, then the upper three teeth would have been deposited between about 35 and 60 ka BP, while the lower sample would have been deposited between about 60 and 100 ka BP.

The LU ESR age estimate for Layer 10 (81 ± 9 ka BP) lies within late OIS 5b or warm-phase 5a (*c.* 90–71 ka BP). This result is consistent with the proposed timing of the cave breaching event, resulting from wave erosion during a high sea level phase of OIS 5. Waves probably carried sediment into the newly exposed cave, and additional sand may have entered from nearby exposed beaches during a subsequent cool, lower sea level phase (i.e., OIS 5d, 5b or 4). Similar absolute dates have been obtained on other Ouljian (Last Interglacial) marine terrace sediments along the Atlantic coast of Morocco (Texier *et al.*, 1994; Weisrock *et al.*, 1999). The single $^{230}Th/^{234}U$ determination of 125 ± 10 ka BP on shell from adjoining cemented beach deposits (Stearns & Thurber, 1965) may correspond to the same high sea stand. The ESR results support major accumulation and cementation of the Layer 10 sands and associated fauna during late OIS 5 or OIS 4.

Enamel samples from the overlying Layers 9, 6, and 5 produced nearly identical EU and LU ESR age estimates, as discussed above. All of these dates fall within OIS 3, a period of marked climatic instability according to various proxy data (e.g., Zhao *et al.*, 1995; Petit *et al.*, 1999). This may account for the relatively rapid succession of cool, dry (depositional) and warmer, moister (rubification, carbonate precipitation) episodes recorded in these strata. The close overlap in age estimates for Layers 6 and 5 is consistent with the view that these layers represent a single depositional episode. It is probable that the Aterian archaeological material recovered from these strata derived from a sequence of occupations prior to the reddening and cementation of Layer 5.

The approximate age range for the Aterian occupations at Mugharet el ‘Aliya is 35–60 ka BP. Due to its meagerness and questionable provenience, the artefact assemblage from Layer 9 should probably be excluded from discussions of the Aterian. Stearns (Howe, 1967: 35) had previously reported a range of 31–26 ka BP for Layers 6 and 5 based on correlations between the cave sediments and northern European glacial cycles as they were understood prior to the development of the marine oxygen isotope record. More significantly, the assemblage from Layer 6 had been assigned to the “Full” (Howe, 1967) or “Final” (Debénath *et al.*, 1986) Aterian phase because of the qualitatively fine craftsmanship of the pedunculates and bifacial foliates and the high frequency of the latter. This assessment related to the typological evolution of the industry proposed by Caton-Thompson (1945), and later reworked for the Maghreb by Antoine (1950). According to their developmental schemes, the latest Aterian assemblages contained the highest proportions and most specialized forms of pedunculates and/or bifacial foliates. If correct, the ESR dates for Layers 6 and 5 imply that the classic Aterian *fossiles directeurs* behave poorly as temporal markers.

The new ESR estimates represent a significant departure from the short Maghreb Aterian chronology of *c.* 40–20 ka BP (e.g., Debénath, 1992; Wengler, 1997) and suggest that the earliest Aterian sites in Morocco probably lie at or beyond the limit of the radiocarbon dating. Figure 4 places the Mugharet el ‘Aliya results alongside published dates for the Aterian in Morocco, organized by material dated and the radiometric method employed (for more detail, see Hawkins, 2001). Many of the published dates are infinite and only a handful may correspond to calendar ages <30 ka BP. Nearly all of the radiocarbon dates are conventional and were obtained from bulk samples of shell or carbonaceous sediment. As Stafford *et al.* (1991) have demonstrated, dates obtained from poorly preserved or minimally pretreated bone consistently underestimate true age relative to dates from collagen or individual amino acids. Delibrias *et al.* (1982) do not identify the

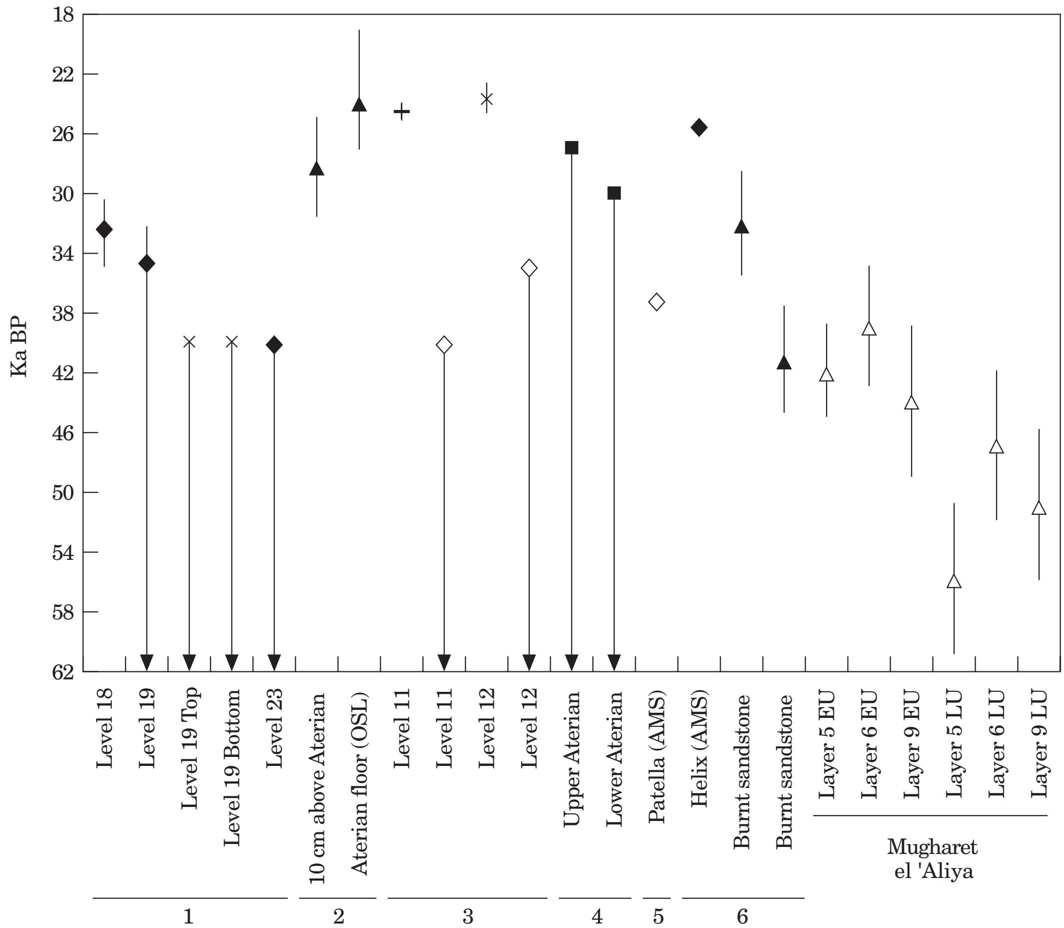

Figure 4. Summary of radiometric dating results from Aterian sites in Morocco. Radiocarbon dates are in uncalibrated radiocarbon ka BP. Dating method symbols: horizontal line: ^{14}C on bone, X: ^{14}C on carbonaceous earth, filled square: ^{14}C on charcoal, filled diamond: ^{14}C on terrestrial shell, empty diamond: ^{14}C on marine shell, filled triangle: TL or OSL, empty triangle: ESR. Sites: 1. Taforalt (Delibrias *et al.*, 1982), 2. Chaperon Rouge (Texier *et al.*, 1988), 3. Grotte des Contrabandiers (Delibrias *et al.*, 1982), 4. Dar es Soltan I (Debénath *et al.*, 1986), 5. Dar es Soltan II (Occhietti *et al.*, 1993), 6. Grotte Zouhrah (Debénath *et al.*, 1986; Occhietti *et al.*, 1993).

bone material (i.e., collagen, apatite, etc.) for the Grotte des Contrabandiers bone date, nor do they define the term “carbonaceous earth” in reference to samples from this site (Level 12) or Taforalt (Level 19 Top and Bottom). Terrestrial and marine shells may continue to exchange carbon with the environment or may undergo recrystallization after the death of the organism. These effects, which can cause significant age underestimation, cannot always be addressed with pretreatment. In addition, oceanic ^{14}C reservoir corrections must be considered for marine shell (Aitken, 1990). As Beck *et al.* (2001) have recently indicated, correction of radiocarbon ages older than about 30 ka BP is made difficult by great instability in atmospheric ^{14}C levels largely attributable to fluctuations in the carbon cycle. Based on earlier correction criteria (e.g., Mazaud *et al.*, 1991), radiocarbon dates in this range are 3–6 ka younger than their true ages. Thus, the published Aterian chronology should probably be considered minimal in most cases because of the materials dated, unclear pretreatment, and/or problems with estimating true age. In most cases, information on sample context, condition, and pretreatment provided in the Aterian date publications is simply too limited to effectively evaluate age reliability.

Conclusion

Stratigraphic and ESR dating evidence indicate that the el ‘Aliya cavity was breached by wave activity during an OIS 5 high sea stand. Layer 10 was deposited by eolian transport of beach sands during a cooler, low sea level phase of late OIS 5 or OIS 4. Significant overlap in ESR ages implies that deposition of Layers 9–5 and weathering of Layers 9 and 5 occurred fairly rapidly. The variable environmental conditions responsible for the lithology of these layers are consistent with short-term climatic vacillations and instability documented during OIS 3. Because the enamel samples were taken from a museum collection and their placement in the cave deposits had to be reconstructed, some uncertainty is introduced with respect to dose rate calculation. However, figures in the Howe (1967) monograph, archive records held at the Peabody Museum, and a visit by one of us (PJW) to the site in April, 2000 permitted reasonable estimation of roof thickness, sediment distribution and sample location. Accounting for variation with moisture content, the Aterian Layers 6 and 5 date between 35 and 60 ka BP, with a broader EU-LU spread for the Layer 5 sample due to higher U content.

The Aterian levels at Mugharet el 'Aliya are too old to provide support for an African origin for the Solutrean of the Iberian peninsula, despite suggestive geographic proximity and some similarities in artefact typology (see Bouzouggar *et al.*, in prep.), but they also do not completely preclude Aterian-Solutrean connections. The existing Moroccan Aterian chronology rests mostly on unreliable radiocarbon dates, and further datings of other sites by AMS or other radiometric techniques will be necessary to determine the latest extent of the industry. The Mugharet el 'Aliya ESR results do indicate an arrival of Aterian foraging groups, or a Mousterian-to-Aterian transition, in Morocco prior to 40 ka BP. This conclusion corresponds well with the early Aterian chronology of the Central Sahara, based on the ^{230}Th/^{234}U record of lake episodes and new TL and OSL results from the Tadrart Acacus (*c.* 90–60 ka BP) (Cremaschi *et al.*, 1998).

Acknowledgements

The ESR dating work was supported by funds from the American School of Prehistoric Research and by a research grant from the Natural Sciences and Engineering Research Council of Canada. We thank Gloria Greis at the Peabody Museum for access to the Mugharet el 'Aliya collection and archive files. Steve Kuhn and three anonymous reviewers provided helpful comments on the manuscript. PJW thanks Ofer Bar-Yosef, Tonya Largy and Richard Meadow for logistical support, Bruce Howe for a first-hand account of the Mugharet el 'Aliya excavations, and Jean-Jacques Hublin, Maxine Kleindienst, Rebecca Miller, Teresa Steele, and especially Alicia Hawkins for useful discussions about the Aterian. WJR thanks J. Johnson for assistance with the sample preparation. This research was supported in part by an NSF Graduate Research Fellowship to PJW.

References

Aitken, M. J. (1990). *Science-based dating in archaeology*. London: Longman.

Alouane, M. J. (1997). Le Quaternaire marin du Cap Achakar (Tanger, Maroc): néotectonique et lithostratigraphie. *Journal of African Earth Sciences* **25,** 391–405.

Antoine, M. (1950). Notes de préhistoire marocaine, XIX – L'Atérien du Maroc atlantique, sa place dans la chronologie nord-africaine. *Bulletin de la Société de Préhistoire du Maroc, Nouvelle série* **1,** 5–47.

Barton, R. N. E., Currant, A. P., Fernandez-Jalvo, Y., Finlayson, J. C., Goldberg, P., Macphail, R., Pettitt, P. B. & Stringer, C. B. (1999). Gibraltar Neanderthals and results of recent excavations in Gorham's, Vanguard and Ibex Caves. *Antiquity* **73,** 13–23.

Beck, J. W., Richards, D. A., Edwards, R. L., Silverman, B. W., Smart, P. L., Donahue, D. J., Hererra-Osterheld, S., Burr, G. S., Calsoyas, L., Jull, A. J. T. & Biddulph, D. (2001). Extremely large variations of atmospheric ^{14}C concentration during the last glacial period. *Science* **292,** 2453–2457.

Binford, L. R. (1979). Organization and formation processes: looking at curated technologies. *Journal of Anthropological Research* **35,** 255–273.

Boëda, E., Geneste, J.-M. & Meignen, L. (1990). Identification des chaînes opératoires lithiques du paléolithique ancien et moyen. *Paleo* **2,** 43–79.

Bordes, F. (1976–77). Moustérien et Atérien. *Quaternaria* **19,** 19–34.

Bouzouggar, A., Kozowski, J. K. & Otte, M. (in prep.). Etude des ensembles lithiques Atériens de la grotte d'el Aliya à Tanger.

Brennan, B. J., Rink, W. J., Rule, E. M., Schwarcz, H. P. & Prestwich, W. V. (1999). The Rosy ESR Dating Program. *Ancient TL* **17,** 45–53.

Brumby, S. (1992). Regression analysis of ESR/TL dose-response data. *Nuclear Tracks and Radiation Measurements* **20,** 595–599.

Caton-Thompson, G. (1945). The Aterian industry: its place and significance in the Palaeolithic world. *Journal of the Royal Anthropological Institute of Great Britain and Ireland* **76,** 87–130.

Clark, J. D. (1993). The Aterian of the Central Sahara. In (L. Krzyzaniak, M. Kobusiewicz & J. Alexander, Eds) *Environmental Change and Human Culture in the Nile Basin and Northern Africa until the Second Millennium B.C.* Poznan: Poznan Archaeological Museum, pp. 49–67.

Coon, C. (1957). *The Seven Caves*. New York: Knopf.

Cremaschi, M., Di Lernia, S. & Garcea, E. A. A. (1998). Some insights on the Aterian in the Libyan Sahara: chronology, environment, and archaeology. *African Archaeological Review* **15,** 261–286.

Debénath, A. (1992). Hommes et cultures matérielles de l'Atérien marocain. *L'Anthropologie* **96,** 711–720.

Debénath, A., Raynal, J-P., Roche, J., Texier, J.-P. & Ferembach, D. (1986). Stratigraphie, habitat, typologie et devenir de l'Atérien marocain: données récentes. *L'Anthropologie* **90,** 233–246.

Delibrias, G., Guillier, M.-T. & Labeyrie, J. (1982). GIF natural radiocarbon measurements IX. *Radiocarbon* **24,** 291–343.

Fontes, J.-Ch. & Gasse, F. (1991). PALHYDAF (Palaeohydrology of Africa) program: objectives, methods, major results. *Palaeogeography, Palaeoclimatology, Palaeoecology* **84,** 191–215.

Gilman, A. (1975). The later prehistory of Tangier, Morocco. *American School of Prehistoric Research Bulletin* **29,** 1–181.

Grün, R. & Stringer, C. B. (1991). Electron spin resonance dating and the evolution of modern humans. *Archaeometry* **33,** 153–199.

Hawkins, A. (2001). Getting a handle on tangs: defining the Dakhleh Unit of the Aterian technocomplex – a study in surface archaeology from Dakhleh Oasis, Western Desert, Egypt. Ph.D. Thesis. University of Toronto.

Howe, B. (1967). The Palaeolithic of Tangier, Morocco. *American School of Prehistoric Research Bulletin* **22,** 1–200.

Howe, B. & Movius, H. L. (1947). A Stone Age cave site in Tangier: preliminary report on the excavations at the Mugharet el 'Aliya, or High Cave, in Tangier. *Papers of the Peabody Museum of American Archaeology and Ethnology, Harvard University* **28,** 1–40.

Hublin, J.-J. (1993). Recent human evolution in northwestern Africa. In (M. J. Aitken, C. B. Stringer & P. A. Mellars, Eds) *The Origin of Modern Humans and the Impact of Chronometric Dating*. Princeton: Princeton University Press, pp. 118–131.

Hublin, J-.J., Barroso Ruiz, C., Medina Lara, O., Fontugne, M. & Reyss, J.-L. (1995). The Mousterian site of Zafarraya (Andalucia, Spain): dating and implications on the Palaeolithic peopling processes of western Europe. *Comptes Rendus de l'Académie des Sciences de Paris, Série II* **321,** 931–937.

Mazaud, A., Laj, C., Bard, E., Arnold, M. & Tric, E. (1991). Geomagnetic field control of ^{14}C production of the last 80 ky: implications for the radiocarbon time-scale. *Geophysical Research Letters* **18,** 1885–1888.

Minugh-Purvis, N. (1993). Reexamination of the immature hominid maxilla from Tangier, Morocco. *American Journal of Physical Anthropology* **92,** 449–461.

Occhietti, S., Raynal, J.-P., Pichet, P. & Texier, J.-P. (1993). Aminostratigraphie du dernier cycle climatique au Maroc atlantique, de Casablanca à Tanger. *Comptes Rendus de l'Académie des Sciences de Paris, Série II* **317,** 1625–1632.

Otte, M. (1997). Contacts trans-méditerranéens au Paléolithique. In (J. M. Fullola & N. Soler, Eds) *El món mediterrani després del Pleniglacial (18.000–12.000 BP)*. Girona: Sèrie Monogràfica 17, Museu d'Arqueologia de Catalunya, pp. 29–39.

Pericot, L. (1942). *La cueva del Parpalló*. Madrid: Diputacíon de Valencia y Consejo Superior de Investigaciones Cientificas (Instituto Diego Veláquez).

Petit, J. R., Jouzel, J., Barkov, N. I., Barnola, J.-M., Basile, I., Bender, M., Chappellaz, J., Davis, M., Delaygue, G., Delmotte, M., Kotlyakov, V. M., Legrand, M., Lipenkov, V. Y., Lorius, C., Pépin, L., Ritz, C., Saltzman, E. & Stievenard, M. (1999). Climate and atmospheric history of the past 420,000 years from the Vostok ice core, Antarctica. *Nature* **399,** 429–436.

Prescott, J. R. & Hutton, J. T. (1988). Cosmic ray and gamma ray dosimetry for TL and ESR. *Nuclear Tracks and Radiation Measurements* **14,** 223–227.

Rink, W. J. (1997). Electron spin resonance (ESR) dating and ESR applications in Quaternary science and archaeometry. *Radiation Measurements* **27,** 975–1025.

Rink, W. J. & Hunter, V. A. (1998). Densities of modern and fossil dental tissues: significance to ESR dating of tooth enamel. *Ancient TL* **15,** 20–28.

Şenyürek, M. S. (1940). Fossil Man in Tangier. *Papers of the Peabody Museum of American Archaeology and Ethnology, Harvard University* **16,** 1–27.

Stafford, T. W., Hare, P. E., Currie, L., Jull, A. J. T. & Donahue, D. J. (1991). Accelerator radiocarbon dating at the molecular level. *Journal of Archaeological Science* **18,** 35–72.

Stearns, C. E. & Thurber, D. L. (1965). Th 230–U 234 dates of late Pleistocene marine fossils from the Mediterranean and Moroccan littorals. *Quaternaria* **7,** 29–41.

Straus, L. G. (2001). Africa and Iberia in the Pleistocene. *Quaternary International* **75,** 91–102.

Texier, J.-P., Huxtable, J., Rhodes, E., Maillier, D. & Ousmoi, M. (1988). Nouvelles données sur la situation chronologique de l'Atérien du Maroc et leurs implications. *Comptes Rendus de l'Académie des Sciences de Paris, Série II* **307,** 827–832.

Texier, J.-P., Lefevre, D. & Raynal, J.-P. (1994). Contribution pour un nouveau cadre stratigraphique de formations littorales Quaternaires de la région de Casablanca (Maroc). *Comptes Rendus de l'Académie des Sciences de Paris, Série II* **318,** 1247–1253.

Weisrock, A., Occhietti, S., Hoang, C.-T., Lauriat-Rage, A., Brebion, P. & Pichet, P. (1999). Les séquences littorales Pléistocènes de l'Atlas atlantique entre Cap Rhir et Agadir, Maroc. *Quaternaire* **10,** 227–244.

Wendorf, F. & Schild, R. (1992). The Middle Paleolithic of Northeast Africa: A status report. In (F. Klees & R. Kuper, Eds) *New Light on the Northeast African Past*. Köln: Heinrich-Barth-Institut, pp. 39–78.

Wengler, L. (1985–86). Chronostratigraphie et préhistorie du Quaternaire récent du Maroc oriental. *Travaux de la Mission Préhistorique et Paléontologique Française au Maroc* **1,** 131–174.

Wengler, L. (1997). La transition du Moustérien à l'Atérien. *L'Anthropologie* **101,** 448–481.

Wrinn, P. J. (in prep.). Reanalysis of Pleistocene archaeofaunas from Mugharet el 'Aliya, Tangier, Morocco: Implications for the Aterian.

Yang, Q., Rink, W. J. & Brennan, B. (1998). Experimental determination of beta attenuation in planar dose geometry and applications to ESR dating of tooth enamel. *Radiation Measurements* **29,** 663–671.

Zhao, M., Beveridge, N. A. S., Shackleton, N. J., Sarnthein, M. & Eglinton, G. (1995). Molecular stratigraphy of cores off northwest Africa: sea surface temperature history over the last 80 ka. *Paleoceanography* **10,** 661–675.